Corner Displacement from Motion Blur

Giacomo Boracchi, Vincenzo Caglioti
Politecnico di Milano
Dipartimento di Elettronica ed Informazione
Via Ponzio, 34/5- 20133 Milano
{giacomo.boracchi, vincenzo.caglioti} @polimi.it

Abstract

We propose a novel procedure for estimating blur in a single image corrupted by blur due to a rigid camera motion during the exposure. Often this blur is approximated as space invariant, even if this assumption holds, for example, only on small image region in perspective images captured during camera movement.

Our algorithm analyzes separately selected image regions containing a corner and in each region the blur is described by its direction and extent. The algorithm works directly in space domain, exploiting gradient vectors at pixels belonging to the blurred corner edges.

The algorithm has been successfully tested both on synthetic and real images showing good performance even on small image regions and in presence of noise.

1 Introduction

Pixel motion estimation is a relevant issue for both image processing and computer vision, as it is often required as a preprocessing step in several algorithms. When there is a significant displacement between the camera and the scene during the exposure, this results in a blur in the acquired image. The blur heavily corrupts image quality and the interpretation of such phenomena is a challenging problem.

Sometimes, the observer can exploit a few images capturing the same scene, or images produced by hybrid imaging systems that, for example, employ simultaneously two cameras [1] or acquire sequentially two images varying the exposure [17]. Clearly, when a single image is available, the problem becomes more complicated and it is usually simplified by assumptions on image blur or exploiting some a priori information on the original image.

Algorithms that pair blur estimation and restoration from a single image (blind deblurring) have been widely studied in the last decades, [4],[5],[12]. Recently, Fergus *et al.* [7] proved good performances in camera shake removal from a single blurred photograph by using a gaussian mixture prior for the distribution of gradient norms. Additionally, they assume the blur uniform on the image, as most of deconvolution based algorithms do. Levin [13] proposed a deblurring method based on image segmentation in (few) areas having the same motion blur extent, but again, the estimated blur direction is considered uniform on the whole image.

Motion estimation from a single blurred image has been addressed for several purposes other than deblurring: the estimation of the optical flow [20], its the integration in a tracking system [10], the measurement of vehicles [14] and balls speed [15] or scene depth [16]. Klein [11] recently proposed a gyroscope based a camera and the measurement of blur produced by rotations.

This paper introduce novel algorithm to estimate space varying blur in a single image, assuming that the relative motion between the camera and the scene produces "smears" i.e. image pixels are blurred along line segments and smears direction and extent are varying between the image pixels. It is the case of indoor environments, where depicted objects have various depth levels, captured by a camera which is "rigidly" moving, as well as scenes acquired by a camera which is rotating around axis parallel to the image plane and passing trough the viewpoint.

The proposed algorithm analyzes image blur only at regions that contains a corner. At blurred corners in fact, the aperture problem does not hold, contrarily to blurred edges (see Figure $1(a)$ regions B and C). At the same time, image corners can be easily detected and modeled. Moreover, corners often correspond to boundaries between scene objects, and therefore they are relevant for motion understanding. Therefore our algorithm is able to analyze images where the blur is space varying, as every region is separately taken into account.

Boracchi and Caglioti [3] recently introduced an algorithm for estimating motion parameters from a blurred corner which works under restrictive hypothesis on motion direction. Such an algorithm was a priori unable to estimate blur parameters at every blurred corners (e.g region D Fig-

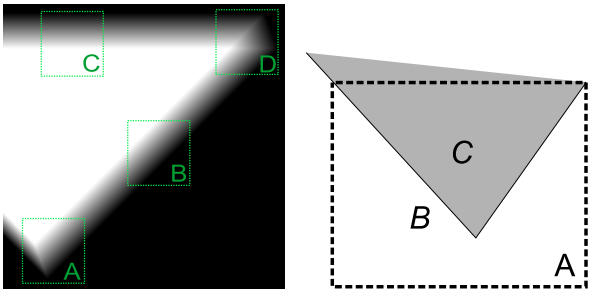

(a) Synthetic blurred corner. (b) The corner model.

Figure 1.

ure $1(a)$). In this paper we present a novel algorithm that extends its capabilities to any image region containing a corner.

2 Problem Formulation

The blurred image I is modeled as

$$I(\mathbf{x}) = K\big(y(\mathbf{x}) + \xi(\mathbf{x})\big) + \eta(\mathbf{x})\,, \quad \mathbf{x} = (x_1, x_2) \qquad (1)$$

being $\mathbf{x}$ a multi index representing image coordinates varying on the discrete domain X, y the original (and unknown) image and K the blur operator. Two sources of gaussian white noise are considered $\xi \sim N(0, \sigma_\xi)$ and $\eta \sim N(0, \sigma_\eta)$; η represents the electronic and the quantization noise, ξ introduces differences between real image corners and the binary corner model used in our algorithm and presented in Section 2.2.

2.1 The Blur Model

The blur operator is, in its more general form, is [2]

$$K\big(y(\mathbf{x})\big) = \int_X k(\mathbf{x}, \mathbf{s}) y(s) ds\,. \qquad (2)$$

Usually K is assumed space invariant and equation (2) becomes a convolution with a point spread function (psf) v:

$$K\big(y(\mathbf{x})\big) = \int_X v(\mathbf{x} - s) y(s)\, ds \; = (v \star y)(\mathbf{x})\,. \qquad (3)$$

This assumption is too restrictive as scene points usually follow different trajectories with respect to the camera viewpoint and this result in different blur in the image. Equation (3) does not describe, for instance, scenes containing several moving objects, scenes with a moving target on a still background or non planar scenes captured by a moving camera.

On the other hand, solving (2) is a difficult inverse problem: to reduce its complexity the blur operator K is locally approximated as a shift invariant blur, i.e.
$\forall \mathbf{x}_0 \in X, \exists\, U_0 \subset X\,,\; x_0 \in U_0$ and a psf v_0 such that

$$K\big(y(\mathbf{x})\big) \approx \int_X v_0(\mathbf{x} - s) y(s) ds \quad \forall \mathbf{x} \in U_0\,. \qquad (4)$$

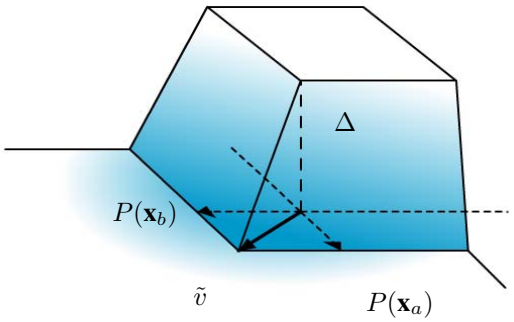

Figure 2. Image in region A, Figure $1(a)$.

Furthermore, only motion blur psf defined over an 1-D linear support are taken into account. These can be written as

$$v_0 = R_{(\theta)}\big(s_l\big)(\mathbf{x}) \quad \theta \in [0, 2\pi], l \in \mathbb{N}$$

$$s_l(x_1, x_2) = \begin{cases} 1/(2l+1), & -l \le x_1 \le l \\ & x_2 = 0 \\ 0, & else \end{cases}$$

where θ and l are motion direction and extent respectively and $R_{(\theta)}\big(s_l\big)$ is s_l rotated by θ degrees on X.

2.2 The Corner Model

Let y be a gray scale image, and $A \subset X$ be a region containing a corner, then the image presents a *binary corner* if $y(A) = \{b, c\}$, where b and c are image intensity values for the background and the corner, respectively. Moreover, $B = y^{-1}(\{b\})$ and $C = y^{-1}(\{c\})$, the sets of pixels belonging to the background and to the corner, have to be separated by two straight segments (having a common endpoint); see Figure 1(b).

Corners in real images are far from being similar to these binary corners. It is reasonable to expect corners to be distinguishable from their background, but hardly they would be uniform. Often their intensities are varying, for example, because of texture, shading or details. Therefore another source of noise ξ has been introduced to add a random component to the binary corner model. As the observed image I is blurred, there should not be a big difference between a blurred image, with the underlying corner not exactly binary and a blurred binary corner with ξ added.

3 Problem Solution

The local maxima of Harris measure [8] are often used to detect image corners, this measure is commonly used in many feature detection algorithms ([18] and references therein). Given a squared region A, see Figure $1(a)$, the set of considered pixels is $D_0 \subset A\;, D_0 = \{\mathbf{x}\; s.t.\; ||\nabla I(\mathbf{x})|| > T\}$, being $T > 0$ a

threshold and ∇I the image gradient defined by two derivatives filters d_1, d_2,

$$\nabla I(\mathbf{x}) = \begin{bmatrix} (I \star d_1)(\mathbf{x}) \\ (I \star d_2)(\mathbf{x}) \end{bmatrix} = \begin{bmatrix} \big((K(y+\xi)+\eta) \star d_1\big)(\mathbf{x}) \\ \big((K(y+\xi)+\eta) \star d_2\big)(\mathbf{x}) \end{bmatrix}. \tag{5}$$

In such a way pixels belonging to flat areas, as well as pixels whose intensity variations are not significant (and eventually due only to η), are not considered. Threshold T is tuned according to η standard deviation, σ_η, which can be estimated from the blurred image [6], [9],[19].
Estimating blur parameters is then equivalent to estimating the displacement vector $\tilde{v}$, i.e. the vector having the same direction of the psf and the norm equal to the blur extent in the considered image region. The displacement vector then, up to its orientation, describes the motion of the image corner during the exposure. Since there is no way to distinguish among the initial and the final corner position from a single blurred image, the motion direction θ ranges between 0 and π. Figure 2 shows $\tilde{v}$ in a blurred corner.

In Figure 2, $\Delta = |b - c|$ is the intensity difference between the corner and the background. Here Δ is assumed to be known, then in Section 4, a procedure for estimating Δ from the blurred region is presented. The noise sources η and ξ are here neglected, while in Section 5 some consideration to cope with them are presented.

The geometrical relations between vectors of Figure 2 yield:

$$\nabla K\big(y(\mathbf{x})\big) \cdot \tilde{v} = \begin{cases} 0, & \text{if } \nabla K\big(y(\mathbf{x})\big) \perp \tilde{v} \\ \pm\Delta, & \text{else} \end{cases}, \forall \mathbf{x} \in D_0\,, \tag{6}$$

and the projection of $\tilde{v}$ along gradient direction, is

$$P(\mathbf{x}) = \frac{\nabla I(\mathbf{x})}{||\nabla I(\mathbf{x})||^2}\Delta\,, \quad \forall \mathbf{x} \in D_0\,. \tag{7}$$

Then, if $\mathbf{x}_a, \mathbf{x}_b \in D_0$ are linearly independent, the displacement vector are obtained by back-projection from $P(\mathbf{x}_a)$ and $P(\mathbf{x}_b)$. When $P(\mathbf{x}_a)$ and $P(\mathbf{x}_b)$ are linearly dependent, the motion direction can not be estimated. This happens when $\mathbf{x}_a$ and $\mathbf{x}_b$ belong to the same blurred edge, where all gradients have the same direction (see Figure 1(a), regions B and C).

As pointed out before, there is no way to exploit motion orientation from a single image, then the orientation of the vectors $P(\mathbf{x})$ can not be used to estimate displacement vector $\tilde{v}$. Given $P(\mathbf{x}_a)$ and $P(\mathbf{x}_b)$, there are four possible displacements vectors: two pairs having the same directions and opposite orientations, as illustrated in Figure 4.

4 Selection of best projection vectors

Consider an image region A containing a binary corner and assume that η and ξ are null. Denote by $\nabla K\big(y\big)(\mathbf{x}_a)$ and $\nabla K\big(y\big)(\mathbf{x}_b)$ the gradient vectors at pixels belonging to the two blurred edges, and by $P(\mathbf{x}_a)$ and $P(\mathbf{x}_b)$ the projections of $\tilde{v}$ along their directions. If the considered image region is large enough, the highest peaks in the 2-D histogram of $\{\nabla I(\mathbf{x}_i)\}_{\mathbf{x}_i \in D_0}$ represent the end points of $\nabla K\big(y\big)(\mathbf{x}_a)$ and $\nabla K\big(y\big)(\mathbf{x}_b)$, then $P(\mathbf{x}_a)$ and $P(\mathbf{x}_b)$ are promptly obtained from (7).

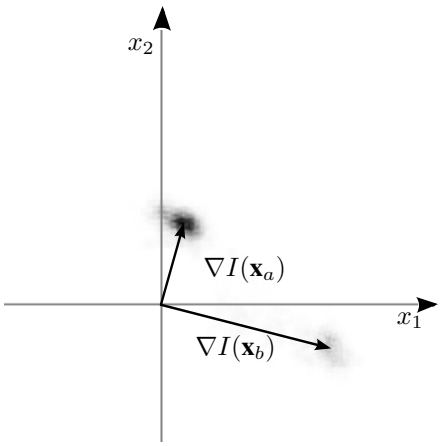

Figure 3. 2d histogram of gradient.

Let now examine how η and ξ affects vectors $\nabla I(\mathbf{x})$. If η and ξ are white noise, according to (1) and (5),

$$\nabla\eta(\mathbf{x}) = \begin{bmatrix} (\eta \star d_1)(\mathbf{x}) \\ (\eta \star d_2)(\mathbf{x}) \end{bmatrix}, \nabla\xi(\mathbf{x}) = \begin{bmatrix} ((\xi \star v) \star d_1)(\mathbf{x}) \\ ((\xi \star v) \star d_2)(\mathbf{x}) \end{bmatrix}, \tag{8}$$

it follows that $E[\nabla\eta + \nabla\xi] = 0$ and, as η and ξ are gaussian distributed, also $\nabla\eta$ and $\nabla\xi$ are also gaussian distributed. Therefore the average of all gradient vectors for pixels belonging to the same blurred edge is an unbiased estimator for $\nabla K\big(\mathbf{x}_a\big)$ or $\nabla K\big(\mathbf{x}_b\big)$.

Figure 3 presents the 2D histogram of $\nabla I(\mathbf{x}), \mathbf{x} \in D_0$. There are two clusters, clearly distinguishable, as the gradient vectors are orthogonal to the corner edges. Since $\nabla\eta$ and $\nabla\xi$ are gaussian distributed, the two most frequent gradient vectors in the 2-D histogram are taken as $\nabla I(\mathbf{x}_a)$ and $\nabla I(\mathbf{x}_b)$ (possibly imposing a minimum angular distance between them). Then formula (7) gives $P(\mathbf{x}_a)$ and $P(\mathbf{x}_b)$ even if their orientations have to be neglected, see Figure 4.

For corners like the one of region D Figure 1(a) there is a third cluster of vectors in the histogram, corresponding to the gradient in the triangular shaped area between the corner blurred edges. If the region containing such corners is big enough, the number of pixels belonging to each of the two blurred edges is larger than the number of pixels in the triangular area. This should be not taken as the projection vector, but, if the corner have not been accurately located in the image, this triangular area may yield uncorrect blur estimates.

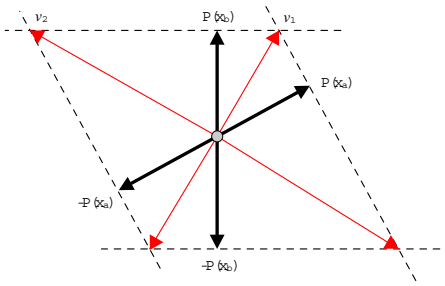

Figure 4. $P(\mathbf{x}_a)$ **and** $P(\mathbf{x}_b)$ **give both** $\tilde{v}_1$ **and** $\tilde{v}_2$**.**

5 Decision Function

Due to the fact that $\tilde{v}$ orientation is unknown, both orientations of $P(\mathbf{x}_a)$ and $P(\mathbf{x}_b)$ have to be considered so that there are two possible solutions, $\tilde{v}_1$ and $\tilde{v}_2$ (see Figure 4). The decision function disambiguates which one, between $\tilde{v}_1$ and $\tilde{v}_2$, is, up to its orientation, the true displacement vector.

Loosely specking, blurred corners can be divided in two classes, according to the presence of gradients whose direction is orthogonal to the true displacement vector. The first class contains corners like the one represented in Figure $1(a)$ region D, having a set of pixels $Z_i = \{\mathbf{x} \in D_0\,,\, \nabla I(\mathbf{x}) \perp \tilde{v}_i\}$. An example of corners of the second class is reported in Figure $1(a)$ region A. For a binary corner of the second class holds $Z_i = \emptyset\,, i = 1$ or $i = 2$ and therefore the number of pixels having gradient orthogonal to each candidate displacement vector (i.e $\#Z_i$) can be taken as discriminant between the two classes. For a binary corner of the first class, $\#Z_i$ corresponds to the surface of a triangle between the two blurred edges, whose value S_1 (S_2) can be calculated from $\tilde{v}_1$ ($\tilde{v}_2$) and N_1 (N_2). If $\#Z_1$ ($\#Z_2$) corresponds to S_1 (S_2), then $\tilde{v}_1$ ($\tilde{v}_2$) is taken as the true displacement vector.

The condition $\nabla I(\mathbf{x}) \perp \tilde{v}$, is relaxed in order to manage camera images and is replaced by

$$\#\{\mathbf{x} \in D_0\,,\, \frac{\nabla I(\mathbf{x}) \cdot \tilde{v}}{|\nabla I(\mathbf{x})||\tilde{v}|} < t\} < S_i \quad i = 1, 2 \qquad (9)$$

where t represent the cosine of a threshold angle between the two vectors. Whenever both $\tilde{v}_1$ and $\tilde{v}_2$ satisfy (9), the one having the largest value in left side of (9) is taken.

Whenever neither $\tilde{v}_1$ and $\tilde{v}_2$ satisfy (9), the corner belongs to the second class. In this case, the derivative along motion direction is constant in D_0, i.e $\nabla I \cdot \tilde{v} = const\ \forall \mathbf{x} \in D_0$. This yields in formula (6) or $+\Delta$, or $-\Delta$, and the signum does not change in the region. Then, the histogram of directional derivatives along directions of $\tilde{v}_1$ and $\tilde{v}_2$ are computed and the more peaked one is selected. The sample kurtosis is taken as peakedness measure.

Finally, in order to obtain a reliable estimate of the motion extent, an accurate estimate of $\Delta = |b - c|$ is required, as Δ scales both $P(\mathbf{x}_a), P(\mathbf{x}_b)$ (see Figure 2). Δ is obtained as the intensity difference between the two highest local maxima in the histogram of image intensities in the region. Since there should be a clear difference between b and c, a minimum distance of half of the intensity range in the region is required.

6 Experiments

Experiments on Synthetic Images: synthetic images have been generated according to equation (1) using the original image y satisfying the binary corner model of Section 2.2 having an angle of $90, 60$, and 45 degrees. The original image is constantly 0 at background and 255 at corner pixels. Blur is produced by a convolution with point spread function having extent $l \in \{20, 30, 40\}$ pixels, and direction $\theta \in \{0, 15, 75, 90\}$ or $\theta \in \{0, 20, 60, 80\}$ according to corners edges orientation.

For each value of blur direction and extent a squared region of 100 pixels, taken around the harris measure maxima (see Figure 5), has been analzed. Images have been corrupted by noise ξ with standard deviation $\sigma_\xi \in \{4, 8, 12, 16\}$ and by η with standard deviation $\sigma_\eta \in \{1, 2, 3, 4\}$, according to equation (1).

Values reported Tables 6 - 3 are $\|v - \tilde{v}\|/\|v\|$ i.e. the distance, in pixels, between the estimated displacement vector $\tilde{v}$, and the true one v, expressed as a percentage with respect to true motion extent. Results have been averaged on 10 realization of η for each value of σ_η and on all directions and extents.

As σ_η, and σ_ξ increases, the decision function may fail to select the true displacement vector: this occurred in about 2.3% of cases.

Experiment on a Test Image: cameraman test image has been blurred by a convolution with a point spread function having direction 35 degrees and length 15 pixels. Then a squared region of 40 pixels centered in every corner selected by an Harris corner detector have been analyzed with our method. Figure 6 shows the blurred cameraman image and the corner displacement vectors estimated. The dashed regions surrounding some of them are the regions where the estimated displacement vector $\tilde{v}$, is less than 2 pixels distant from the vector having point spread function parameters. The average error in the correct matches is 0.71 pixels. The algorithm results are accurate in regions containing a corner satisfy the model presented in Section 2.2. The regions where the algorithm fails do not contain a binary corner.

Experiment on Camera Images: a triplet of camera images have been captured according to the following scheme. First a still image at the initial camera position is taken, followed by a blurred image captured moving the camera during the exposure. At the end of the exposure, another still image at the final camera position, is taken. In this way the

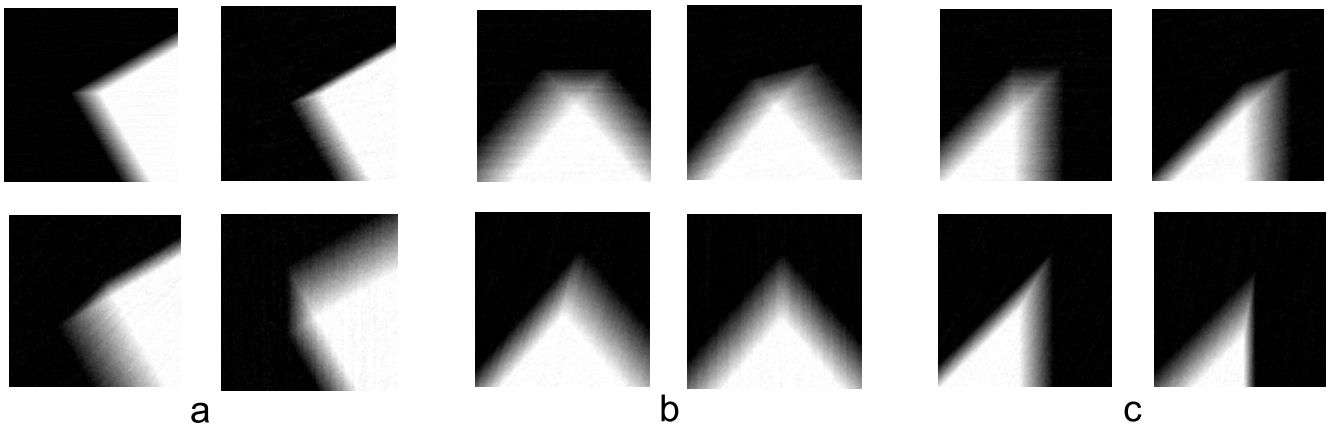

Figure 5. Examples of Synthetic Test Images from dataset.

Figure 6. Cameraman synthetically blurred.

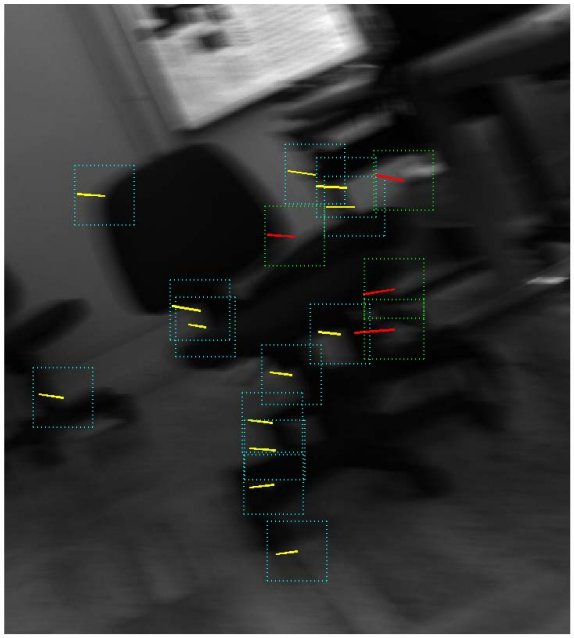

Figure 7. Test on real image.

algorithm performance on a real motion blurred image is be compared with the ground truth obtained by matching the two still images. Again, the corners have been selected by local maxima of Harris measure and a region of 50 pixels around each of them have been analyzed (camera images were actually bigger than camera images).

Figure 7 shows the blurred camera picture and the regions where $\tilde{v}$ was less than 7 pixels distant from the displacement vector estimated by matching [21] the features in the corresponding region in the initial and final images. The average error in the correct matches is 4.84 pixels. Finally in the regions where the displacement vectors is marked in red, the decision function discards the displacement vector closer to the true displacement vector parameters (this happens 4 times over 17).

7 Discussion and Ongoing Works

The experiments show that the blurred corners have been suitably modeled and that is possible to estimate the blur even in a small image region containing a corner. The algorithm represent an improvement with respect to the optical flow estimation procedure proposed in [20], as motion analysis is performed at interesting region, not on a fixed image tessellation. We believe that spatial domain procedure are more suited to blur analysis as do not impose restriction on region size with respect to psf length, while Fourier transform based methods do. Moreover, specifically at corners, Fourier coefficients are heavily influenced by the presence of corner edges, so that blur parameters estimation is harder.

$\sigma_\eta \mid \sigma_\xi$	4	8	12	16
1	1.77 %	1.73 %	1.53 %	1.48 %
2	1.97 %	2.00 %	1.91 %	2.05 %
3	2.52 %	2.76 %	2.58 %	2.61 %
4	3.35 %	3.64 %	3.60 %	3.69 %

Table 1. Result on corner of Figure 5a, $l \in \{20, 30, 40\}$ pixels, $\theta \in \{0, 15, 75, 90\}$

$\sigma_\eta \mid \sigma_\xi$	4	8	12	16
1	2.50 %	2.33 %	2.31 %	2.66 %
2	2.71 %	2.77 %	2.86 %	3.13 %
3	3.44 %	3.61 %	3.82 %	3.75 %
4	4.89 %	4.39 %	4.84 %	5.03 %

Table 2. Result on corner of Figure 5b, $l \in \{20, 30, 40\}$ pixels, $\theta \in \{0, 15, 75, 90\}$

$\sigma_\eta \mid \sigma_\xi$	4	8	12	16
1	1.87 %	1.9 %	1.83 %	1.86 %
2	1.97 %	1.9 %	1.88 %	1.94 %
3	2.53 %	2.3 %	2.27 %	2.29 %
4	3.18 %	3.1 %	2.99 %	3.12 %

Table 3. Result on corner of Figure 5a, $l \in \{20, 30, 40\}$ pixels, $\theta \in \{0, 20, 60, 80\}$

Ongoing works concern a procedure to filter the corners found by the Harris detector in order to process exclusively regions containing a blurred corner. We are also working on a refinement of the decision function, to increase its reliability with camera images. Finally, we believe that, as there are no restriction on region shape, a considerable improvement in robustness would be given by adaptively selecting every corner region. This method can be used in initialization of deblurring algorithm assuming space varying blur, such as [22], which requires user supervision during initialization.

References

[1] M. Ben-Ezra and S. Nayar. Motion based motion deblurring. *IEEE Transactions on Pattern Analysis and Machine Intelligence*, 26(6):689–698, Jun 2004.

[2] M. Bertero and P. Boccacci. *Introduction to Inverse Problems in Imaging*. Institute of Physics Publishing, 1998.

[3] G. Boracchi and V. Caglioti. Motion blur estimation at corners. In *Inproceedings of VISAPP 2007 Conference, Barcelona*, 2007.

[4] T. Cannon. Blind deconvolution of spatially invariant image blurs with phase. *ASSP*, 24(1):58–63, February 1975.

[5] T. Chan and C. Wong. Total variation blind deconvolution. *IEEE Transaction on Image Processing*, 7(3):370–375, March 1998.

[6] D. L. Donoho and I. M. Johnstone. Ideal spatial adaptation by wavelet shrinkage. *Biometrika*, 81(3):425–455, 1994.

[7] R. Fergus, B. Singh, A. Hertzmann, S. T. Roweis, and W. T. Freeman. Removing camera shake from a single photograph. *ACM Trans. Graph.*, 25(3):787–794, 2006.

[8] C. Harris and M. Stephens. A combined corner and edge detector. In *Proceedings of the 4th Alvey Vision Conference,*, pages 147–151, 1988.

[9] J. Immerkær. Fast noise variance estimation. *Computer Vision and Image Understanding*, 64(2):300–302, 1996.

[10] S. Kawamura, K. Kondo, Y. Konishi, and H. Ishigaki. Estimation of motion using motion blur for tracking vision system. In *World Automation Congress, 2002. Proceedings of the 5th Biannual*, volume 13, pages 371–376, 9-13 June 2002.

[11] G. Klein and T. Drummond. A single-frame visual gyroscope. In *Proc. British Machine Vision Conference (BMVC'05)*, volume 2, pages 529–538, Oxford, September 2005. BMVA.

[12] D. Kundur and D. Hatzinakos. Blind image deconvolution. *SPMag*, 13(3):43–64, May 1996.

[13] A. Levin. Blind motion deblurring using image statistics. In B. Schölkopf, J. Platt, and T. Hoffman, editors, *Advances in Neural Information Processing Systems 19*. MIT Press, Cambridge, MA, 2007.

[14] H.-Y. Lin. Vehicle speed detection and identification from a single motion blurred image. *wacv-motion*, 01:461–467, 2005.

[15] H.-Y. Lin and C.-H. Chang. Automatic speed measurements of spherical objects using an off-the-shelf digital camera. In *Mechatronics, 2005. ICM '05. IEEE International Conference on*, pages 66–71, 10-12 July 2005.

[16] H.-Y. Lin and C.-H. Chang. Depth recovery from motion blurred images. *icpr*, 1:135–138, 2006.

[17] M. V. Marius Tico. Estimation of motion blur point spread function from differently exposed image frames. In *Proceedings of Eusipco 2006, 4-6 September 2006 Florence, Italy*, 2006.

[18] K. Mikolajczyk, T. Tuytelaars, C. Schmid, A. Zisserman, J. Matas, F. Schaffalitzky, T. Kadir, and L. V. Gool. A comparison of affine region detectors. *International Journal of Computer Vision*, 65(1/2):43–72, 2005.

[19] S. Olsen. Noise variance estimation in images, proc. 8th scia, troms, norway, may 25-28, 1993.

[20] I. M. Rekleitis. Steerable filters and cepstral analysis for optical flow calculation from a single blurred image. In *Vision Interface*, pages 159–166, Toronto, May 1996.

[21] P. H. S. Torr and D. W. Murray. Outlier detection and motion segmentation. In P. S. Schenker, editor, *Sensor Fusion VI*, pages 432–443. SPIE volume 2059, 1993. Boston.

[22] M. Welk, D. Theis, and J. Weickert. Variational deblurring of images with uncertain and spatially variant blurs. In *DAGM-Symposium*, pages 485–492, 2005.